Draft version March 16, 2023
Typeset using LaTeX **twocolumn** style in AASTeX631

Search for Ultra-High-Energy Neutrinos from Binary Black Hole Mergers with the Pierre Auger Observatory

The Pierre Auger Collaboration

(Dated: March 16, 2023)

ABSTRACT

The Pierre Auger Observatory is sensitive to ultra-high-energy (UHE) neutrinos of energies above ~ 0.1 EeV. The time- and direction-dependent sensitivity of the Pierre Auger Observatory makes it also a suitable instrument for searches of transient sources. Here, we present a search for UHE neutrinos from binary black hole (BBH) mergers that have been observed through the emission of gravitational waves (GWs). We have performed the search for two different hypothetical emission periods after each merger: 24 hours and 60 days. By accounting for the time-dependent exposure to neutrinos emitted from 3D localization probability distributions provided by LIGO/Virgo, we probe the UHE-neutrino luminosity assuming a universal luminosity for all mergers with an E_ν^{-2} spectrum and constant emission throughout these periods as a benchmark model. As no neutrinos have been identified in coincidence with the BBH mergers, we constrain their UHE-neutrino luminosity based on the observational parameters. The corresponding limit on the total energy emitted in UHE neutrinos per source is $\sim 2.3 \cdot 10^{53}$ erg (at 90% C.L.). This limit does not depend strongly on the search duration. Additionally, we compare our results to previous bounds and present the sensitivity of the stacking method as a function of time after the merger which can be of interest to constrain other emission models.

Keywords: High energy astrophysics, Neutrino astronomy, Ultra-high-energy neutrinos, Transient sources, Gravitational wave sources, Astrophysical black holes

1. INTRODUCTION

After the detection of the first direct GW signal from a BBH merger by LIGO, GW150914 (Abbott et al. 2016a), the LIGO and Virgo Collaborations (LVC) carried out a total of three observational runs (O1, O2, and O3) (Abbott et al. 2018). In O2, the first GW signal from a binary neutron star merger, GW170817, was detected, accompanied by an unprecedented multi-wavelength and multi-messenger observation and search campaign (Abbott et al. 2017) featuring a rich variety of observations that remain unique to date, such as that of a kilonova (Arcavi et al. 2017). Part of this campaign was also the follow-up search for high and ultra-high-energy (UHE) neutrinos (Albert et al. 2017), where no neutrino candidates with significant temporal and directional correlation have been observed, leading to constraints in the astrophysical parameter space of the source. In addition, the detections of GW signals from 83 BBH mergers, the most prevalent type of GW events found in O1 through O3, have been published by LVC (Abbott et al. 2019, 2021a,b,c). Together, they represent a new class of astrophysical transients which has not yet been observed by any other means than their GW emission, such that any further observations or constraints could lead to new insights on their properties.

Ultra-high-energy cosmic ray (UHECR) production in BBH mergers, which could also lead to UHE photon and neutrino production, has been the subject of theoretical work (Kotera & Silk 2016; Perna et al. 2016; Anchordoqui 2016; Bartos et al. 2017). Electromagnetic signals coincident with BBH mergers have been detected, however none of them was significant enough to claim a discovery (Connaughton et al. 2016, 2018; Graham et al. 2020). As a contribution to the large set of multi-messenger follow-up searches of BBH mergers, a dedicated search program for UHE photons and neutrinos from BBH mergers with the Pierre Auger Observatory has been implemented, with no UHE-neutrino candidates identified. This work focuses on UHE neutrinos. A limit of UHE photons is the subject of a separate publication (Abdul et al. 2023). UHE neutrinos, in contrast to UHE photons, reach Earth from virtually arbitrary

distances without being absorbed, allowing to probe potential sources also in the distant Universe.

The capability of the Pierre Auger Observatory to detect and identify UHE neutrinos has been demonstrated and discussed in previous works concerning searches for a diffuse UHE-neutrino flux (Aab et al. 2019a) and UHE-neutrino point sources (Aab et al. 2019b). In the latter, we have reported the sensitivity to UHE neutrinos in a declination range from $-90°$ to $+60°$, covering well above 90% of the whole sky. However, the sensitivity across the field of view is far from uniform. It is much larger close to the horizon, leading to strongly enhanced sensitivity to transient sources for the case that they are located in the corresponding directions. A good example is the follow-up search of GW170817 (Albert et al. 2017), which was located in the most sensitive region directly below the horizon at the time of the merger, allowing us to set very stringent UHE-neutrino limits in particular for short-term emission. Other published UHE neutrino limits from point sources using the Pierre Auger Observatory include the first two reported BBH mergers (Aab et al. 2016) and the neutrino-emitting blazar TXS 0506+056 (Aab et al. 2020). In the present work, we utilize the UHE-neutrino detection capability of the Pierre Auger Observatory to combine it with the observational parameters of a large set of BBH mergers detected by LVC, which we stack to constrain their UHE-neutrino emission given the absence of neutrino candidates.

2. LIGO/VIRGO BINARY BLACK HOLE MERGER EVENTS

The BBH merger events followed up in this work originate from three different sets:

1. The GW event catalog GWTC-1 (Abbott et al. 2019), containing high-confidence GW events from the LIGO/Virgo runs O1 and O2. All events except the binary neutron star merger GW170817 from GWTC-1 are classified as BBH mergers.

2. The GW event catalog GWTC-2 (Abbott et al. 2021a) and its update GWTC-2.1 (Abbott et al. 2021b), containing GW events from the LIGO/Virgo run O3 from 1 April 2019, 15:00 UTC through 1 October 2019, 15:00 UTC. This part of O3 is commonly referred to as O3a. Following the argument in Abbott et al. (2021a), all events in these catalogs with an inferred mass of the lighter coalescing object $m_2 < 3M_\odot$ are not in accordance to the BBH merger hypothesis and are therefore excluded. Furthermore, only high-confidence astrophysical events that are most likely originating from BBH mergers are taken into account. This is done by requiring the inferred probability of a BBH merger origin, $P_{\rm BBH}$, to be larger than 0.5, following the selection criterion in Abbott et al. (2021b).

3. The GW event catalog GWTC-3 (Abbott et al. 2021c), containing GW events from O3b, the part of the LIGO/Virgo run O3 between 1 November 2019, 15:00 UTC and 27 March 2020, 17:00 UTC. Analogous to GWTC-2 and GWTC-2.1, we consider all events with $P_{\rm BBH} > 0.5$ and $m_2 > 3M_\odot$.

In total, this selection leads to 83 BBH merger events being considered for this work.

For each selected BBH merger event, the following source parameters from the catalogs are used:

1. The signal detection time t_0 of the merger

2. The directional localization probability density function (PDF), given in terms of a probability ρ_p for each of the pixels p of a discrete healpix skymap (Calabretta & Roukema 2007) normalized such that $\sum_p \rho_p = 1$, where the sum is taken over all pixels in the skymap

3. The luminosity distance PDF Π_p, given for each individual pixel p in the healpix skymap. It is parameterized in terms of a luminosity distance parameter $r_{_L}$ such that $\int_0^\infty \Pi_p(r_{_L})\,{\rm d}r_{_L} = 1$ for each pixel p. The parameterization Π_p is a shifted normal distribution times $r_{_L}^2$ as documented in Singer et al. (2016).

The latter two PDFs comprise the 3D localization.

For each event in GWTC-1, we are using the parameter estimation skymaps provided in Abbott et al. (2021d), which are unambiguous. For each event in GWTC-2 and GWTC-2.1, several parameter estimations have been provided for each source (Abbott et al. 2021a; LIGO Scientific Collaboration, & Virgo Collaboration 2021). For GWTC-2, this includes a suitable combination of posterior samples, called "PublicationSamples" as explained in Zevin et al. (2021), which we use for this work, while for the additional events provided in GWTC-2.1, we use the parameter estimation "PrecessingSpinIMRHM_comoving", following the suggestion from the example notebook provided in LIGO Scientific Collaboration, & Virgo Collaboration (2021). For GWTC-3, parameter estimations from a mixture of the most commonly applied techniques are used, named "PEDataRelease_cosmo_reweight_C01:Mixed" in LIGO Scientific Collaboration, Virgo Collaboration, KAGRA Collaboration (2021).

3. ULTRA-HIGH-ENERGY NEUTRINO SEARCHES WITH THE PIERRE AUGER OBSERVATORY

The Pierre Auger Observatory (Aab et al. 2015a) is the largest observatory for cosmic rays in the world. It covers an area of 3000 km^2 at 35° 12′ S, 69° 19′ W in the province of Mendoza, Argentina, at a mean altitude of 1400 m above sea level. It comprises a surface detector (SD) (Allekotte et al. 2008), which is an array of 1660 water-Cherenkov detectors ("stations") with 1.5 km spacing, sampling the particles of extensive air showers at the ground level. In the following, in most cases, "the SD" and "the Pierre Auger Observatory" are interchangeable as the SD is the main component of the Pierre Auger Observatory that we use for this work.

Although the primary goal of the SD is to detect UHECRs, it can also identify UHE neutrinos. There are two classes of neutrino events that the SD is able to detect: down-going neutrinos of all flavors interacting in the atmosphere and inducing extensive air showers (EASs); and Earth-skimming τ neutrinos that undergo charged-current weak interactions inside the Earth, producing τ leptons, which exit the Earth and decay in the atmosphere, inducing slightly up-going EASs. Both the down-going and the up-going EASs induced by neutrinos can be distinguished from those induced by UHECRs due to their reduced shower age: As they start closer to the detector than UHECR-induced EASs of similar geometries, they contain a substantial electromagnetic component. This causes significantly longer signals in the SD stations compared to the short signals from the muons that are the main remaining component at the ground from UHECR-induced air showers at the considered angles (zenith angle $\theta > 60°$). The UHE-neutrino searches are optimized to distinguish these signal traces in a direction-dependent manner via the ratios of their time-integrals to their maximum values. This allows to efficiently and strongly separate UHE-neutrino showers from those induced by UHECRs, leading to a sensitive and reliable UHE-neutrino identification (Aab et al. 2019a).

To quantify the direction-dependent sensitivity to UHE neutrinos, the effective area $A_{\rm eff}$ as a function of the local zenith angle and neutrino energy is used. It is defined via the following relation between the rate of detected neutrino events and the neutrino energy spectral flux ϕ_ν:

$$\frac{\mathrm{d}N_\nu(\theta,t)}{\mathrm{d}t} = \int_0^\infty \phi_\nu(E_\nu)\, A_{\rm eff}(E_\nu,\theta,t)\, \mathrm{d}E_\nu \,. \quad (1)$$

It is discussed in detail together with further properties of the direction dependence of the UHE-neutrino sensitivity in Aab et al. (2019b). The explicit time dependence of the effective area at a fixed zenith angle originates from individual SD stations not being available at all times and from short periods in which the data quality of the SD has been found to be insufficient (Abraham et al. 2010). For the calculations in this work, we always account for this variation of $A_{\rm eff}$ based on time-dependent detector status information.

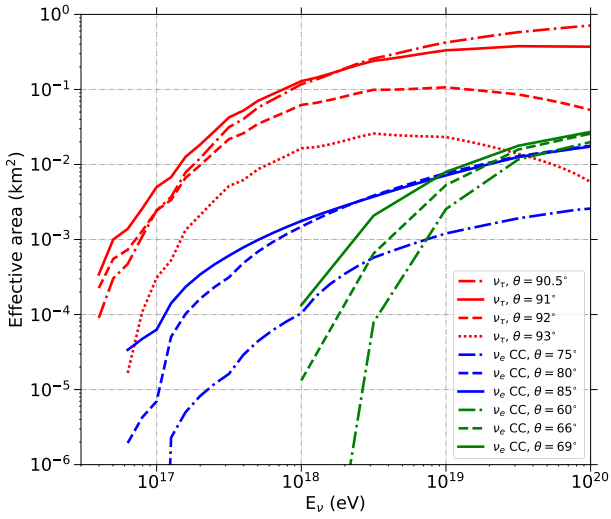

Figure 1. The neutrino effective area $A_{\rm eff}$ of the SD of the Pierre Auger Observatory for various zenith angles, averaged over the year 2016.

The average of $A_{\rm eff}$ over the year 2016, i.e. the benchmark given in Aab et al. (2019b), is shown in Figure 1 as a function of neutrino energy for various zenith angles. For down-going directions ($\theta < 90°$), $A_{\rm eff}$ is always increasing with energy due to the increase of the shower dimensions and also of the neutrino-nucleon cross section. At the highest energies this increase is however not very rapid. For some of the Earth-skimming zenith angles, in particular for $\theta > 91°$, $A_{\rm eff}$ as a function of energy has a maximum, after which it decreases with energy. This is because the Earth itself becomes opaque to neutrinos due to the large amount of traversed matter, meaning that any further increase of the energy decreases its survival probability and therefore also the probability of an eventual detection. Another reason is that the τ lepton decay length increases linearly with energy, causing τ leptons at the highest energies to decay too high above the ground for the resulting showers to be detectable on the ground. The overall behavior of $A_{\rm eff}$ as a function of zenith angle is discussed below based on Figure 2.

For this work, UHE-neutrino energy spectra are assumed to be $\phi_\nu \propto E_\nu^{-2}$, which is a common benchmark assumption for neutrino analyses at the highest energies. Analogous approaches for other forms of the spectrum are possible by adapting the calculations in this work

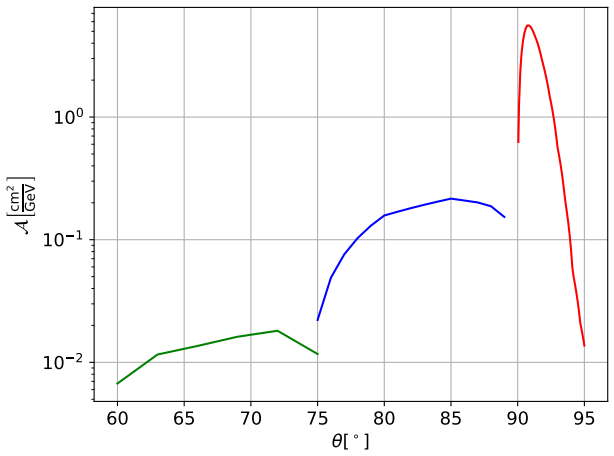

Figure 2. The 2016 average of the neutrino effective area folded with the assumed $\propto E_\nu^{-2}$ neutrino energy spectrum. Colors correspond to the colors in Figure 1, indicating different angular ranges, for which there are distinct analyses as discussed in Aab et al. (2019b).

accordingly. The integral of $A_{\rm eff}$ over the E_ν^{-2} spectrum can be factorized in the calculation of the number of neutrino events (see below) to give the spectrum weighted effective area:

$$\mathcal{A}(\theta, t) = \int_0^\infty E_\nu^{-2}\, A_{\rm eff}(E_\nu, \theta, t)\, \mathrm{d}E_\nu \ . \qquad (2)$$

The expected rate of detected neutrinos is proportional to $\mathcal{A}$, which is shown in Figure 2 as a function of the zenith angle, using the benchmark $A_{\rm eff}$ from Figure 1. It will be used later in this work to calculate the relation between neutrino emission at the sources and expected number of detected neutrinos.

As could be inferred already from the zenith dependence of the effective area $A_{\rm eff}$, $\mathcal{A}(\theta)$ increases strongly above 90°. Specifically, it has a high peak at 90.8°, indicating the particularly large sensitivity of the Pierre Auger Observatory to Earth-skimming τ neutrinos. The peak can be explained by a balance between two competing effects of neutrino interactions inside the Earth: very close to the horizon ($\theta = 90°$), not enough matter is traversed such that neutrinos are unlikely to interact at all; too far from the horizon, neutrinos interact very deep inside the Earth, preventing an eventual detection of an air shower at the surface of the Earth. The properties and dependencies of neutrino-induced air shower detection are discussed in more detail in a general manner in Zas (2005) and focused on detection with the Pierre Auger Observatory in Aab et al. (2019b).

4. ULTRA-HIGH-ENERGY NEUTRINO FOLLOW-UP OBSERVATIONS

We have searched for neutrino candidates applying the same selection criteria as in Aab et al. (2015b) in the most probable 90% quantile of the directional localization PDF of each source. The searches have been performed using two emission time windows starting at the time of the merger t_0. The shorter one is 24 hours, as also chosen in Aab et al. (2016). It covers both the expected prompt and afterglow emission durations as discussed in Aab et al. (2016). While it is much longer than the observation period of ±500 s around the merger, which has been used in many previous follow-up works (Aartsen et al. 2014; Adrian-Martinez et al. 2016; Albert et al. 2019; Hussain et al. 2020; Aartsen et al. 2020; Abe et al. 2016, 2021), we present a method of constraining the emission also for short time intervals within the first day after the merger in Section 6. The 500 s previous to each merger have been searched as well with no positive detection. Conservatively, they have not been taken into account for the calculation of the results due to their very small impact. Due to the low background expectation for UHE neutrinos with the Pierre Auger Observatory (Aab et al. 2015b), we additionally searched for UHE neutrinos until 60 days after the mergers to probe even longer emission scenarios (Murase et al. 2016; Kotera & Silk 2016; McKernan et al. 2019). For this search, we expect < 0.05 false positive UHE-neutrino events. It should be noted that these time intervals for observation refer to the time as measured in the comoving reference frame of each source, as explained in the next paragraph. The number of expected background events is hardly affected by this scaling of the observation times and stays well below 0.05 for the whole search.

In this work, we take into account the impact of cosmological redshift on time intervals: Due to time dilation we increase the observation times by factors of $(1 + z_s)$, where z_s is the expectation value of the redshift of each source s. As the spatial configuration of hypothetical neutrino emission regions is highly uncertain, we can not quantify any additional gravitational redshift and thus do not account for it. The impact of the cosmological redshift on particle energies is covered by the luminosity distance parameter in all calculations regarding the distance. All redshifts have been calculated from the luminosity distances based on Wright (2006) for a flat universe assuming $H_0 = 70\ \mathrm{km\,s^{-1}\,Mpc^{-1}}$ for the Hubble constant and $\Omega_m = 0.3$ for the matter density parameter.

The follow-up observations were performed automatically, utilizing the GCN notices and skymaps containing the localization PDFs given by LVC as described before. In the automatic search procedure, reconstructed

air shower events that do not lie within the follow-up time window and inside the most probable 90% quantile of the directional PDF of the respective GW source are discarded.

No events were found after applying the time, direction, and neutrino selection criteria. This allows us to determine limits on the UHE-neutrino emission as calculated in the following section.

5. CONSTRAINTS ON THE ULTRA-HIGH-ENERGY-NEUTRINO EMISSION OF BINARY BLACK HOLE MERGERS

In this work, we constrain the emission in terms of the UHE-neutrino luminosity of the sources, in contrast to other works presenting limits on the flux of neutrinos at Earth (Albert et al. 2017; Aab et al. 2019b). For our benchmark approach, we assume a universal and constant UHE-neutrino luminosity for all BBH mergers with a spectral neutrino emission rate given by $k\,E_\nu^{-2}$. The neutrinos are assumed to be emitted isotropically during the period of the chosen duration, starting at the time of the merger.

For a specific point source located at a given luminosity distance r_L, the corresponding flux at Earth would be $\phi_\nu = k\,E_\nu^{-2} \,/\, (4\pi r_L^2)$. Here the normalization constant k can be simply related to the UHE-neutrino luminosity through $L_{\mathrm{UHE}\nu} = k\,\ln(E_2 \,/\, E_1)$, where E_1 is the lowest and E_2 the highest UHE-neutrino energy that contributes to $L_{\mathrm{UHE}\nu}$. Specifically, the values are $E_1 = 10^{17}$ eV and $E_2 = 2.5 \cdot 10^{19}$ eV. They correspond to the energy range containing the upper 90% of the UHE-neutrino sensitivity to an E_ν^{-2} flux (Aab et al. 2019a). We could also have chosen a different energy range. Since we constrain $L_{\mathrm{UHE}\nu}$ only indirectly via k, the value of the result would simply change proportionally to $\ln(E_2 \,/\, E_1)$ of the chosen energy range.

We do not impose any *a priori* weights on the UHE-neutrino luminosity as a function of time nor as a function of the astrophysical or geometrical properties of the sources, such as the emitted energy in terms of GWs, the spin parameters of the two black holes or the relative orientation of the orbiting system with respect to the GW detectors. It should be noted that this is an over-simplification that only serves as a benchmark for potential further studies, in which more elaborate models could be probed.

The calculation is based on the total number of neutrinos $N_{\mathrm{UHE}\nu}$ that can be expected to be collected from all the sources, only taking into account observational parameters related to the source position and its luminosity distance. The cumulative number of expected neutrinos can be written as a sum over the sources (characterized by subindex "s") of the integral of the spectral flux at Earth and the effective area of the Pierre Auger Observatory to neutrinos, A_{eff}, over neutrino energy and time. As the precision of the localization in the sky is limited, each possible arrival direction (discretized over pixels with index "p") is weighted by the PDF, $\rho_{p,s}$ (see Section 2). Similarly, the PDF of the luminosity distance for each discretized direction, $\Pi_{p,s}(r_L)$, is used to weight the attenuation factor, $(4\pi r_L^2)^{-1}$ in an integral over luminosity distance, r_L. Finally, the contribution to the flux from each source is weighted by the probability that the LVC has assigned to the GW event originating from a BBH merger, $P_{\mathrm{BBH},s}$, so that the final result reads:

$$N_{\mathrm{UHE}\nu} = \sum_s P_{\mathrm{BBH},s} \sum_{p\in\Omega_{90}(s)} \rho_{p,s} \int_0^\infty \Pi_{p,s}(r_L)\frac{k}{4\pi r_L^2}\,\mathrm{d}r_L \times \int_{t_0}^{t_0+T_s}\int_0^\infty E_\nu^{-2}\,A_{\mathrm{eff},p}(E_\nu,t)\,\mathrm{d}E_\nu\,\mathrm{d}t\,. \tag{3}$$

Here, the time integration starts at the detection of the merger, t_0, and lasts for the search duration interval $T_s = T(1+z_s)$ in the Earth's system, with T being 24 hours or 60 days, in accordance to our follow-up observations described in Section 4. The sum over the possible localization of each BBH merger is limited to a solid angle $\Omega_{90}(s)$, within which one finds the most probable 90% quantile of the directional localization PDF of the source s. This corresponds to our procedure of discarding all SD events outside of this region. For $P_{\mathrm{BBH},s}$, the highest value determined in any of the LVC search procedures, or *pipelines*, for the respective source s is taken, corresponding to the most confident detection of the source. For most of the sources regarded in this work, $P_{\mathrm{BBH},s}$ is very similar for all pipelines that lead to a detection, meaning that the result is barely dependent on the choice of the pipeline. We identify the factorized energy integral $\int_0^\infty E_\nu^{-2}\,A_{\mathrm{eff},p}(E_\nu,t)\,\mathrm{d}E_\nu = \mathcal{A}_p(t)$ introduced in Equation (2) and plotted in Figure 2 as a function of arrival zenith angle. A_{eff} depends on the zenith angle, which in turn is determined by the pixel p (observing direction) and the observing time. Most of the time dependence of $\mathcal{A}_p(t)$ arises because the arrival zenith angle for the pixel p depends on detection time, but there is a minor dependence on the status of the array which varies with time.

The non-observation of neutrino candidates with a background low enough to be compatible with zero allows us to set the 90% C.L. upper limit $N^{\mathrm{up}}_{\mathrm{UHE}\nu}$ to 2.44 (Feldman & Cousins 1998). We solve Equation (3) for k, which can be converted to a limit on

the UHE neutrino luminosity, $L_{\mathrm{UHE}\nu}$, once E_1 and E_2 are fixed:

$$L^{\mathrm{up}}_{\mathrm{UHE}\nu} = N^{\mathrm{up}}_{\mathrm{UHE}\nu} \ln\left(\frac{E_2}{E_1}\right) \left(\sum_s P_{\mathrm{BBH},s} \sum_{p\in\Omega_{90}(s)} \rho_{p,s} \int_{t_0}^{t_0+T_s} \mathcal{A}_p(t-t_0)\,\mathrm{d}t \int_0^{\infty} \frac{\Pi_{p,s}(r_L)}{4\pi r_L^2}\,\mathrm{d}r_L \right)^{-1} . \quad (4)$$

When this is applied to all the data from the three runs of LVC, amounting to a total of 83 BBH merger events, the obtained limit on the UHE-neutrino luminosity between $E_1 = 10^{17}$ eV and $E_2 = 2.5 \cdot 10^{19}$ eV for an activity period of 24 hours is $2.7 \cdot 10^{48}$ erg s^{-1}. If the chosen period is instead 60 days, the corresponding value is $4.6 \cdot 10^{46}$ erg s^{-1}. Multiplying this luminosity limit by the respective period T, one obtains the limit to the total energy emitted in UHE neutrinos, assuming constant luminosity over the period. Since we are interested in the combined limit in terms of the emission in the reference system of the source, we have to multiply simply by the search duration T at the source, which is not adjusted due to the redshift. The results are $2.3 \cdot 10^{53}$ erg for the 24-hour period and $2.4 \cdot 10^{53}$ erg for 60-day period. The reason why these values are almost the same is the following: One multiplies the luminosity limit by the search duration T, which is proportional to the interval length of time integrals in Equation (4). Thus, a longer period T will result in the luminosity limit being multiplied by a larger factor, while also necessitating a proportionally longer integration interval length in the denominator. The still remaining small difference between the energy limit for the 60-day search and the one for 24 hours lies in the small temporal variations of the SD status.

Naturally, as more data are gathered for the stacking analysis, the limit becomes more restrictive. The result for $L^{\mathrm{up}}_{\mathrm{UHE}\nu}$ for the 24-hour follow-up period for the ten sources of GWTC-1, the first catalog containing events from the runs O1 and O2, is $8.9 \cdot 10^{48}$ erg s^{-1}. When including also GWTC-2.1, which contains the first 41 sources of O3, it becomes $4.3 \cdot 10^{48}$ erg s^{-1}. We note that the luminosity bound does not improve linearly with the number of considered sources. This is because the average distance of the sources has increased from O1 over O2 to O3 due to the improved sensitivity of the LIGO and Virgo gravitational wave detectors.

We can estimate the contributions of individual events to the calculated stacking limit in a simple way by considering the fraction of the expected neutrino flux given in Equation (3) that can be attributed to a given source s. In the limit calculation, the summation over sources appears in the denominator of Equation (4). The weight of each individual BBH merger to the 24-hour limit calculated in this fashion and expressed as a percentage is displayed in Figure 3 for all 83 sources in chronological order. The percentage for each considered GW event assigned to its ID can be found in Table 1 in the Appendix.

We note that the first and third entry correspond to the first two published BBH merger events by the LIGO collaboration, namely GW150914 and GW151226 (Abbott et al. 2016a,b). The non-observation of UHE neutrinos with the Pierre Auger Observatory coincident with these events was addressed in Aab et al. (2016). In the calculation of these limits, the PDFs of the source positions were not considered. The reported limits of the energy emitted in UHE neutrinos were $7.7 \cdot 10^{53}$ erg and $7.9 \cdot 10^{53}$ erg, respectively. These limits are overly optimistic since they are the most stringent limits that could be obtained in the hypothetical case that the source positions were exactly located at the optimal declination that yields the highest sensitivity of the Observatory and assuming the emission lasted for 24 hours (or an integer number of days).

We can clearly see that GW151226 is one of the sources that gives the largest individual contribution to the stacking limit as defined above, almost 10%. In contrast to that, GW150914 has a contribution of about 1.4%. The large discrepancy between the relative weights of these sources might at first glance be surprising, especially when considering that the deduced expectation value of the distance is ~ 400 Mpc for both cases. However, the difference can be well explained by the localization PDFs of the sources: The most probable position of GW151226 has a large overlap with the declination of highest effective area of the Pierre Auger Observatory, while in case of GW150914, the most likely declination lies outside its field of view.

6. TIME-DEPENDENT SENSITIVITY

The sensitivity of the SD to a source changes as it moves through the field of view. This means that the effective area changes significantly over that period, particularly when a source moves just below the horizon and the Earth-skimming channel is activated, which typically happens for a short time each day as the source transits between the zenith angles of 90° and 95°. For the two optimal declination values, $\delta = -54.5°$ and $\delta = 59.5°$, the observable transit time is much longer and the corresponding point source sensitivity is very much enhanced (Aab et al. 2019b). Each source samples different times within a sidereal day after the merging time with a time dependent sensitivity, depending on

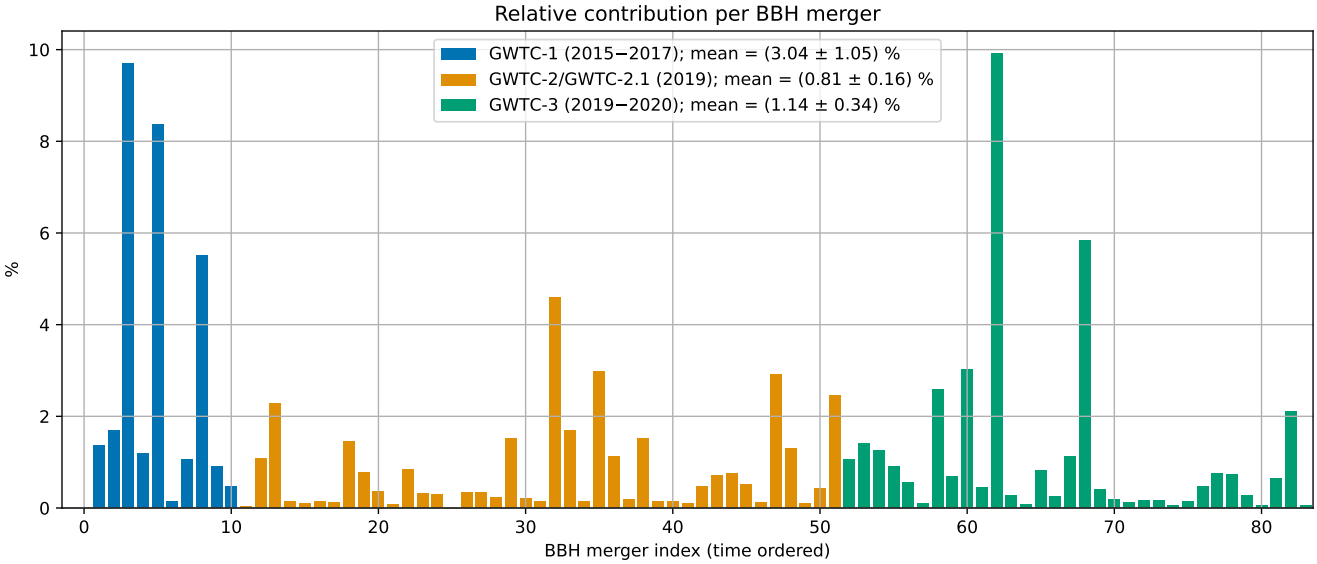

Figure 3. Relative contribution of each BBH merger to the 24-hour UHE-neutrino luminosity limit. BBH mergers are represented in chronological order with colors indicating GW event catalogs. Mean values of the relative contributions per catalog and their statistical uncertainties are given in the legend. Table 1 in the Appendix contains the values of the relative contributions and the corresponding GW event IDs associated to the indices in this plot.

the location of the event in the sky and on the time of the merger.

As more sources are observed and combined, the commonly probed period after the merger is much more uniformly covered than for single events. The way this is achieved can be explored as follows. The limit in Equation (4) is obtained by integrating in time over periods T_s that correspond to a period T of 24 hours or 60 days in the source frame. Since there is a linear conversion between the Earth's frame and each source frame, one could express this integral in terms of the time in the source frame without principal changes. We denote the corresponding time variable t'. Integrating over an interval $\Delta t'$, small relative to the time variability of the exposure, we obtain a neutrino luminosity bound, $L_{\mathrm{UHE}\nu}(t'-t_0)$, that depends on the time after the merger, $t'-t_0$. The resulting value of the limit increases by a factor of order $T\,/\,\Delta t'$ because it is assumed the sources *only* emit neutrinos at time t' and during a short time interval $\Delta t'$. If $\Delta t'$ is much smaller than the true characteristic emission time of the source, the luminosity limit obtained is clearly overestimated. One can circumvent this issue by converting the luminosity to the energy emitted in UHE neutrinos over the interval as in the previous section to obtain $\mathcal{E}_{\mathrm{UHE}\nu}(t'-t_0) = L_{\mathrm{UHE}\nu}(t'-t_0)\Delta t'$. The increase in the flux limit is compensated and the energy limits obtained are directly comparable to those obtained in an arbitrary period, in particular over a sidereal day and 60 days as discussed in Section 5.

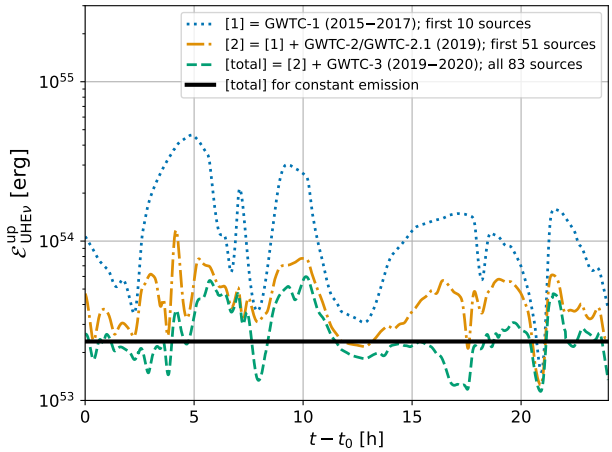

Figure 4. Solid line: upper limit (90% C.L.) on the total energy emitted in UHE neutrinos for an isotropically emitted constant E_ν^{-2} flux for a period of 24 hours as measured at the sources; other lines: analogous upper limit on the emitted energy determined via the observational parameters as a function of time after the merger; the green dashed line corresponds to the full set of sources and the lines above correspond to smaller subsets of sources.

The result for the full set of sources from all catalogs is shown in Figure 4 along with partial results obtained only with the ten events of GWTC-1, and the 51 events of GWTC-2.1 and GWTC-1 combined. The variations with time after the merger in this limit are due to the cumulative effect of the different sampling in $t'-t_0$ for each source of the corresponding catalog,

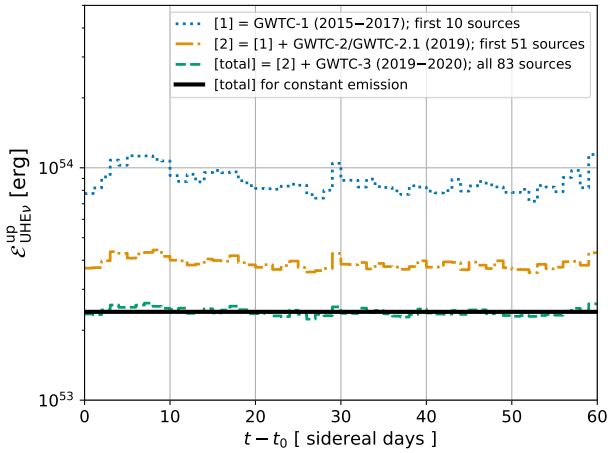

Figure 5. Solid line: upper limit (90% C.L.) on the time-dependent universal isotropic neutrino luminosity for the 60-day follow-up period, averaged per sidereal day in the rest frame of each source; other lines: partial results containing only the given subsets of events.

reflecting both the changing effective area of the detector with time as well as the distance for that particular source. Nearby sources can drive the lowest values of this plot if they have the optimal declination and this happens at a given time $t' - t_0$ after the merger. As an example, the prominent minimum close to 21 hours after the merger is strongly dominated by the contribution of the relatively close-by GW event GW170608, for which the localization PDF has a large overlap with the Earth-skimming field of view of Auger at that time.

It can be appreciated that the limit obtained by combining all runs exhibits smaller variations than the contributions to the limit from just a subset of the sources, as the contributions of all sources are averaged out. The energy limit of $\mathcal{E}^{\rm up}_{\rm UHE\nu} = 2.3 \cdot 10^{53}$ erg obtained for a constant emission during a 24-hour period for the three catalogs described before is indicated as straight solid line and the green dashed curve illustrates how the sensitivity varies in $t' - t_0$ during 24 hours. The plot illustrates how the combination of several sources and different runs substantially improves the sensitivity to BBH mergers as compared to those obtained with single events or partial catalogs.

Similarly, we can plot the limits on the energy emitted in neutrinos during the 60-day period after the merger. This plot would display daily variations close to those in Figure 4 which would be difficult to see. Figure 5 displays instead the 24-hour limit for each successive day after the event. The plot illustrates the stability of the time-dependent limit over the 60-day search period, both for the overall limit, as well as for the contributions of the partial catalogs. Again, it is clear how the increase in the number of stacked sources makes the upper bound more stable as different periods of observation average out the fluctuations due to the SD status which typically exhibits only slight variations from day to day (Abreu et al. 2011). The plot also displays $\mathcal{E}_{\rm UHE\nu} = 2.4{\cdot}10^{53}$ erg as a straight line, the energy in UHE neutrinos calculated in Section 5 for the 60-day period.

7. DISCUSSION AND CONCLUSIONS

We have presented a stacking search for UHE neutrinos from LIGO/Virgo BBH mergers with the Pierre Auger Observatory. As no UHE-neutrino candidates have been identified in temporal and directional coincidence with any of the BBH mergers, we have obtained a 90% C.L. upper limit on the assumed universal isotropic UHE-neutrino luminosity. It has been obtained in the assumption of a neutrino differential flux $\propto E_\nu^{-2}$, which is a common benchmark assumption for UHE-neutrino searches. The directional coincidence has been probed by applying the search to the most probable 90% quantile of the directional localization PDF of each source. For the first time, we also account for the probabilities of the individual GW signals reported by LIGO/Virgo to originate from BBHs. The temporal coincidence has been probed for two search periods, starting at the time of the merger and lasting for 24 hours and 60 days in the comoving reference frame of each source. Doing that, as a first approach, we make the simple assumption that the sources emit at a constant rate.

The obtained luminosity limits in the neutrino energy range $10^{17}\,\mathrm{eV} - 2.5 \cdot 10^{19}\,\mathrm{eV}$ are $2.7 \cdot 10^{48}$ erg s^{-1} and $4.6{\cdot}10^{46}$ erg s^{-1} for the 24-hours and 60-days period, respectively. These can be easily converted into the corresponding limits on the total energy emitted in neutrinos in the same energy interval, resulting in $2.3 \cdot 10^{53}$ erg and $2.4 \cdot 10^{53}$ erg (at 90% C.L.). These quantities are more robust because they do not depend directly on the assumed duration of the emission. The slight difference in the two values is due to the effective area of the Observatory which has typically small variations due to changes in the SD status. The cumulative effect has been also explored by comparing the emitted energy in neutrinos of all the BBH merger events to those obtained for two partial catalogues, the ten events of GWTC-1, and the 51 events of GWTC-2.1 and GWTC-1 combined. We have also explored the relative contributions of each merger event to the calculation of the expected neutrinos at Earth from all sources. Most objects contribute less than 2% as could be expected, but there are a few events that contribute more than 5%. One of the events that contributes most (about 10%) is GW151226. The results obtained in this work are com-

pared to early calculations of limits to GW150914 and GW151226 obtained with the Pierre Auger Observatory that did not account for the PDF of the source direction.

The instantaneous effective area of the Pierre Auger Observatory is mostly determined by the zenith angle of the event and thus depends on the 3D localization of the source as well as the time of the merger event. Each source is visible for a fraction of the day with a varying effective area. We have also studied the combined sensitivity of the Observatory in the stacking approach as a function of time after the merger. This is done considering emission over a time period which is small compared to the variability of the effective area and calculating the total energy emitted in UHE neutrinos. The limits obtained this way do not depend on the assumed duration of the emission time. The results are shown in Figure 4 for a period of 24 hours after the merger event for the full set of events and two subsets, demonstrating the effect of the stacking. In spite of combining a sizeable number of GW events, the plot still partially reflects some variability of the followed-up sources, which manifests as dips in these curves. This is due to the large directional dependence of the effective area of the Observatory. In Figure 5, we display the bounds of the energy emitted in UHE neutrinos obtained in a similar way, integrating for each successive 24-hour interval for a period of 60 days after the events. As the daily variations are removed, the remaining dependence reflects small changes in the array status.

The limits of the energy emitted in UHE neutrinos can be compared to the energy emitted in GWs. The mean value of the emitted GW energies for all 83 BBH mergers is $\sim 4.9 \cdot 10^{54}$ erg. A comparison to our UHE-neutrino energy limits $\mathcal{E}^{\rm up}_{{\rm UHE}\nu}$ from either search period yields an upper limit on the ratio of the energy emitted in UHE neutrinos to that emitted in GWs of approximately 5%. This is a constraint on the UHE-neutrino production efficiency with the potential to contribute to theoretical considerations such as in Kotera & Silk (2016). However, as we have assumed only a simplified benchmark model, in particular determining only the isotropic equivalent total energy and assuming an E_ν^{-2} spectrum, we note that more elaborate models could yield different results.

Another application utilizing the neutrino energy limits is a comparison to similar searches performed with IceCube (Aartsen et al. 2020; Abbasi et al. 2023), which impose limits in the range of $1.37 \cdot 10^{52}$ erg through $7.18 \cdot 10^{55}$ erg to the same BBH mergers that we consider in this work. As the search by IceCube is focusing on the TeV to PeV energy range, while Auger focuses on EeV energies, the results of this work should be considered as complementary to those of IceCube.

REFERENCES

Aab, A., et al. 2015a, Nucl. Instrum. Meth. A, 798, 172, doi: 10.1016/j.nima.2015.06.058

—. 2015b, Phys. Rev. D, 91, 092008, doi: 10.1103/PhysRevD.91.092008

—. 2016, Phys. Rev. D, 94, 122007, doi: 10.1103/PhysRevD.94.122007

—. 2019a, JCAP, 10, 022, doi: 10.1088/1475-7516/2019/10/022

—. 2019b, JCAP, 11, 004, doi: 10.1088/1475-7516/2019/11/004

—. 2020, Astrophys. J., 902, 105, doi: 10.3847/1538-4357/abb476

Aartsen, M. G., et al. 2014, Phys. Rev. D, 90, 102002, doi: 10.1103/PhysRevD.90.102002

—. 2020, Astrophys. J. Lett., 898, L10, doi: 10.3847/2041-8213/ab9d24

Abbasi, R., et al. 2023, Astrophys. J., 944, 80, doi: 10.3847/1538-4357/aca5fc

Abbott, B. P., et al. 2016a, Phys. Rev. Lett., 116, 061102, doi: 10.1103/PhysRevLett.116.061102

—. 2016b, Phys. Rev. Lett., 116, 241103, doi: 10.1103/PhysRevLett.116.241103

—. 2017, Astrophys. J. Lett., 848, L12, doi: 10.3847/2041-8213/aa91c9

—. 2018, Living Rev. Rel., 21, 3, doi: 10.1007/s41114-020-00026-9

—. 2019, Phys. Rev. X, 9, 031040, doi: 10.1103/PhysRevX.9.031040

Abbott, R., et al. 2021a, Phys. Rev. X, 11, 021053, doi: 10.1103/PhysRevX.11.021053

—. 2021b. https://arxiv.org/abs/2108.01045

—. 2021c. https://arxiv.org/abs/2111.03606

—. 2021d, SoftwareX, 13, 100658, doi: 10.1016/j.softx.2021.100658

Abdul Halim, A., et al. 2023, ApJ, xx, xx. https://arxiv.org/abs/2301.0xxxx

Abe, K., et al. 2016, Astrophys. J. Lett., 830, L11, doi: 10.3847/2041-8205/830/1/L11

—. 2021, Astrophys. J., 918, 78, doi: 10.3847/1538-4357/ac0d5a

Abraham, J., et al. 2010, Nucl. Instrum. Meth. A, 613, 29, doi: 10.1016/j.nima.2009.11.018
Abreu, P., et al. 2011, Astropart. Phys., 34, 368, doi: 10.1016/j.astropartphys.2010.10.001
Adrian-Martinez, S., et al. 2016, Phys. Rev. D, 93, 122010, doi: 10.1103/PhysRevD.93.122010
Albert, A., et al. 2017, Astrophys. J. Lett., 850, L35, doi: 10.3847/2041-8213/aa9aed
—. 2019, Astrophys. J., 870, 134, doi: 10.3847/1538-4357/aaf21d
Allekotte, I., et al. 2008, Nucl. Instrum. Meth. A, 586, 409, doi: 10.1016/j.nima.2007.12.016
Anchordoqui, L. A. 2016, Phys. Rev. D, 94, 023010, doi: 10.1103/PhysRevD.94.023010
Arcavi, I., et al. 2017, Nature, 551, 64, doi: 10.1038/nature24291
Bartos, I., Kocsis, B., Haiman, Z., & Márka, S. 2017, Astrophys. J., 835, 165, doi: 10.3847/1538-4357/835/2/165
Calabretta, M. R., & Roukema, B. F. 2007, Mon. Not. Roy. Astron. Soc., 381, 865, doi: 10.1111/j.1365-2966.2007.12297.x
Connaughton, V., et al. 2016, Astrophys. J. Lett., 826, L6, doi: 10.3847/2041-8205/826/1/L6
—. 2018, Astrophys. J. Lett., 853, L9, doi: 10.3847/2041-8213/aaa4f2
Feldman, G. J., & Cousins, R. D. 1998, Phys. Rev. D, 57, 3873, doi: 10.1103/PhysRevD.57.3873
Graham, M. J., et al. 2020, Phys. Rev. Lett., 124, 251102, doi: 10.1103/PhysRevLett.124.251102
Hussain, R., Vandenbroucke, J., & Wood, J. 2020, PoS, ICRC2019, 918, doi: 10.22323/1.358.0918
Kotera, K., & Silk, J. 2016, Astrophys. J. Lett., 823, L29, doi: 10.3847/2041-8205/823/2/L29
LIGO Scientific Collaboration, & Virgo Collaboration. 2021, GWTC-2.1: Deep Extended Catalog of Compact Binary Coalescences Observed by LIGO and Virgo During the First Half of the Third Observing Run - Parameter Estimation Data Release, v1, Zenodo, doi: 10.5281/zenodo.5117703
LIGO Scientific Collaboration, Virgo Collaboration, KAGRA Collaboration. 2021, GWTC-3: Compact Binary Coalescences Observed by LIGO and Virgo During the Second Part of the Third Observing Run — Parameter estimation data release, Zenodo, doi: 10.5281/zenodo.5546663
McKernan, B., Ford, K. E. S., Bartos, I., et al. 2019, Astrophys. J. Lett., 884, L50, doi: 10.3847/2041-8213/ab4886
Murase, K., Kashiyama, K., Mészáros, P., Shoemaker, I., & Senno, N. 2016, Astrophys. J. Lett., 822, L9, doi: 10.3847/2041-8205/822/1/L9
Perna, R., Lazzati, D., & Giacomazzo, B. 2016, Astrophys. J. Lett., 821, L18, doi: 10.3847/2041-8205/821/1/L18
Singer, L. P., et al. 2016, Astrophys. J. Lett., 829, L15, doi: 10.3847/2041-8205/829/1/L15
Wright, E. L. 2006, Publ. Astron. Soc. Pac., 118, 1711, doi: 10.1086/510102
Zas, E. 2005, New J. Phys., 7, 130, doi: 10.1088/1367-2630/7/1/130
Zevin, M., Bavera, S. S., Berry, C. P. L., et al. 2021, Astrophys. J., 910, 152, doi: 10.3847/1538-4357/abe40e

APPENDIX

A. OBSERVATIONAL PARAMETERS FOR CONSIDERED LIGO/VIRGO BBH MERGER EVENTS

Index	GW event ID	Contrib. [%]	Max. frac. 90% contour in FoV	Index	GW event ID	Contrib. [%]	Max. frac. 90% contour in FoV
1	GW150914	1.35	1.00	41	GW190805_211137	0.11	0.52
2	GW151012	1.70	0.65	42	GW190828_063405	0.47	0.81
3	GW151226	9.71	1.00	43	GW190828_065509	0.71	1.00
4	GW170104	1.19	0.52	44	GW190910_112807	0.76	0.51
5	GW170608	8.36	0.66	45	GW190915_235702	0.51	0.80
6	GW170729	0.13	1.00	46	GW190916_200658	0.12	0.80
7	GW170809	1.05	1.00	47	GW190924_021846	2.92	1.00
8	GW170814	5.50	1.00	48	GW190925_232845	1.30	0.59
9	GW170818	0.90	1.00	49	GW190926_050336	0.10	1.00
10	GW170823	0.46	0.54	50	GW190929_012149	0.43	0.81
11	GW190403_051519	0.03	1.00	51	GW190930_133541	2.45	0.61
12	GW190408_181802	1.07	0.98	52	GW191103_012549	1.05	0.39
13	GW190412	2.29	1.00	53	GW191105_143521	1.41	0.60
14	GW190413_052954	0.13	0.51	54	GW191109_010717	1.26	0.56
15	GW190413_134308	0.10	0.83	55	GW191113_071753	0.90	0.99
16	GW190421_213856	0.14	0.83	56	GW191126_115259	0.56	0.49
17	GW190426_190642	0.11	0.49	57	GW191127_050227	0.10	0.58
18	GW190503_185404	1.45	1.00	58	GW191129_134029	2.58	1.00
19	GW190512_180714	0.78	1.00	59	GW191204_110529	0.69	0.88
20	GW190513_205428	0.37	0.74	60	GW191204_171526	3.02	0.91
21	GW190514_065416	0.07	0.41	61	GW191215_223052	0.44	1.00
22	GW190517_055101	0.83	0.79	62	GW191216_213338	9.91	0.67
23	GW190519_153544	0.32	0.49	63	GW191222_033537	0.27	0.99
24	GW190521	0.29	1.00	64	GW191230_180458	0.09	1.00
25	GW190521_074359	0.00	1.00	65	GW200112_155838	0.82	0.48
26	GW190527_092055	0.33	0.55	66	GW200128_022011	0.24	0.91
27	GW190602_175927	0.33	1.00	67	GW200129_065458	1.12	1.00
28	GW190620_030421	0.22	0.50	68	GW200202_154313	5.83	1.00
29	GW190630_185205	1.51	0.68	69	GW200208_130117	0.40	1.00
30	GW190701_203306	0.21	1.00	70	GW200208_222617	0.18	0.81
31	GW190706_222641	0.14	0.88	71	GW200209_085452	0.12	0.59
32	GW190707_093326	4.58	0.56	72	GW200216_220804	0.16	0.76
33	GW190708_232457	1.68	0.47	73	GW200219_094415	0.16	0.72
34	GW190719_215514	0.14	0.52	74	GW200220_061928	0.05	0.83
35	GW190720_000836	2.99	1.00	75	GW200220_124850	0.14	0.57
36	GW190725_174728	1.12	0.53	76	GW200224_222234	0.47	1.00
37	GW190727_060333	0.19	1.00	77	GW200225_060421	0.74	0.52
38	GW190728_064510	1.51	0.77	78	GW200302_015811	0.73	0.55
39	GW190731_140936	0.14	0.50	79	GW200306_093714	0.27	0.44
40	GW190803_022701	0.13	0.58	80	GW200308_173609	0.06	0.48
				81	GW200311_115853	0.65	1.00
				82	GW200316_215756	2.11	1.00
				83	GW200322_091133	0.05	0.38

Table 1. Observational parameters for the GW events considered in this work; indices correspond to those in Figure 3; column "Contrib. [%]": relative time-integrated contribution of each BBH merger to the total 24-hour limit, i.e. values from Figure 3; column "Max. frac. 90% contour in FoV": maximum fraction of the 90% C.L. localization region in the sky found in the neutrino field of view of the Pierre Auger Observatory during the 24 hours after the merger